www.sciencetranslationalmedicine.org/cgi/content/full/6/255/255ra133/DC1

Supplementary Materials for

Closed-loop neuromodulation of spinal sensorimotor circuits controls refined locomotion after complete spinal cord injury

Nikolaus Wenger, Eduardo Martin Moraud, Stanisa Raspopovic, Marco Bonizzato, Jack DiGiovanna, Pavel Musienko, Manfred Morari, Silvestro Micera, Grégoire Courtine*

*Corresponding author. E-mail: gregoire.courtine@epfl.ch

Published 24 September 2014, *Sci. Transl. Med.* **6**, 255ra133 (2014)
DOI: 10.1126/scitranslmed.3008325

This PDF file includes:

Other Supplementary Material for this manuscript includes the following:
(available at www.sciencetranslationalmedicine.org/cgi/content/full/6/255/255ra133/DC1)

SUPPLEMENTARY METHODS

Surgical procedure and post-surgical care

Surgical interventions were performed under general anesthesia and aseptic conditions. All 8 animals examined in this study exhibited a complete transection of the mid-thoracic spinal cord (~ spinal segment T7). The completeness of the spinal cord transections was verified during surgery by two independent surgeons by lifting the cut ends of the cord (*14*). Gel foam was inserted into the gap created by the transection as a coagulant and to separate the cut ends of the spinal cord. The transections led to permanent and complete paralysis of the hindlimbs in all the tested rats (*n*=8) (Fig. 1C). The spinal cord tissue was kept postmortem for histological evaluations in order to verify lesion completeness (fig. S1). The tissue was stained against glial fibrillary acidic protein (GFAP) and no remaining neural tissue was observed at the site of the lesion.

Stimulating electrodes were created by removing a small part (1 mm notch) of insulation from Teflon-coated stainless steel wires (AS632, Cooner Wire). These were subsequently secured during surgery at the midline overlying spinal level L2 and S1 by suturing the wires to the dura. A common ground wire (1 cm of Teflon removed at the distal end) was inserted subcutaneously over the right shoulder. Bipolar intramuscular EMG electrodes (AS632; Cooner Wire) were implanted using the same wire type, into the tibialis anterior and medial gastrocnemius muscles, bilaterally. All electrode wires were connected to a percutaneous amphenol connector (Omnetics Connector Corporation) cemented to the skull of the rat. The rats then received a complete transection of the spinal cord (~T7). The proper location of the epidural and EMG electrodes was verified post-mortem, along with the extent and location of the lesion.

Kinematic, ground reaction force, and electromyographic recordings

Bilateral hindlimb kinematics were recorded using 12 infrared motion capture cameras (200 Hz; Vicon). Reflective markers were attached bilaterally overlying iliac crest, greater trochanter (hip), lateral condyle (knee), lateral malleolus (ankle) and the distal end of the fifth metatarsal (limb endpoint) (Fig. 1A). Nexus (Vicon) was used to obtain 3D coordinates of the markers. The body was modeled as an interconnected chain of rigid segments, and joint angles were generated accordingly. EMG signals (12.207 kHz) were amplified, filtered (10–5,000-Hz bandpass) and recorded synchronized to kinematic and ground reaction force data. Vertical ground reaction forces were measured using a biomechanical force plate (2 kHz; HE6X6, AMTI) located below the treadmill belt, or along the runway. Video recordings (200

Hz) were obtained using two cameras (Basler Vision Technologies) oriented at 90° and 270° with respect to the direction of locomotion.

A minimum of 10 step cycles was extracted for each experimental condition and rat. A total of 147 parameters quantifying gait, kinematics, ground reaction force, and EMG features were computed for each limb and gait cycle according to methods described in detail previously (*14, 39, 42, 43*). These parameters provide a comprehensive quantification of gait patterns ranging from general features of locomotion to fine details of limb motion. The entire list of 147 computed parameters is described in table S1.

Reflex analysis

EES-evoked motor potentials were recorded in TA and MG muscles. Each pulse of stimulation elicits a medium-latency and late-latency response, which were determined based on their respective latency (*17*), as illustrated in Fig. 4A. The peak amplitude of each response was measured through custom-made software in Matlab. Spectral analysis of EMG activity by fast Fourier transformation (FFT) was performed on the identified bursts of EMG activity recorded from the TA and MG muscles. Spectral peaks in frequency ranges from 0 to 160 Hz were calculated. Burst amplitude was calculated as the mean of the rectified EMG signal during stance and swing phase for MG and TA muscle, respectively. The area under the curve of the rectified EMG signal was calculated separately for the monosynaptic and polysynaptic responses. Both responses were aligned separately along the normalized gait cycle and their response activity calculated using a moving average with a 150 ms window size. Results are reported in percentage of the maximum value across all tested frequencies.

Principal component analysis

The various experimental conditions led to substantial modulation of gait patterns, which were evident in the modifications of a large proportion of the computed parameters. In order to extract the modulated gait characteristics in response to changes in stimulation features, we implemented a multi-step statistical procedure based on principal component (PC) analysis (*14, 42*). PC analyses were applied on data from all individual gait cycles for all the rats together. Data were analyzed using the correlation method, which adjusts the mean of the data to zero and the standard deviation to 1. This is a conservative procedure that is appropriate for variables that differ in their variance (e.g. kinematic vs. EMG data).

SUPPLEMENTARY FIGURES

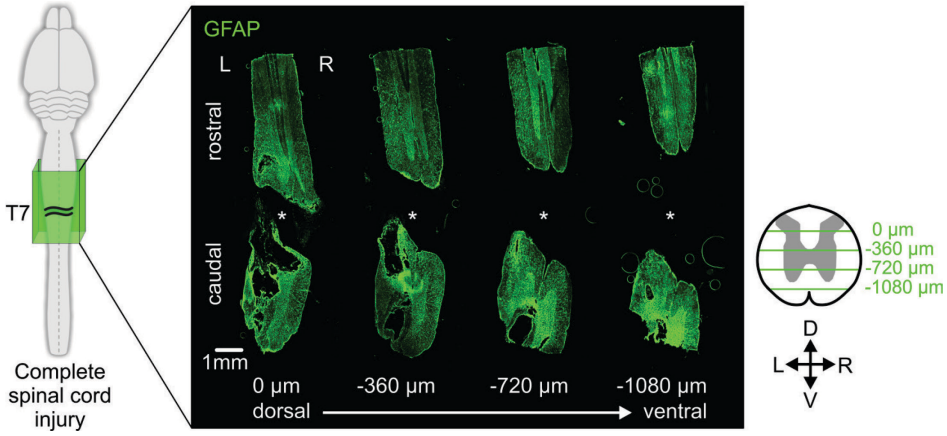

Fig. S1. Completeness of the SCI. Rats received a complete transection of the spinal cord around mid-thoracic segment T7. The completeness and location of the lesion was verified macroscopically during surgery by two independent surgeons, and post-mortem through histological evaluations. The photographs show a series of histological sections stained against glial fibrillary acidic protein (GFAP) in a representative rat. The site of lesion is marked with an asterisk (*). Images were obtained on coronal sections taken at regular intervals (360 µm) from the dorsal to ventral aspects of the spinal cord. Histological slice thickness, 30 µm. L, left; R right; D, dorsal; V, ventral.

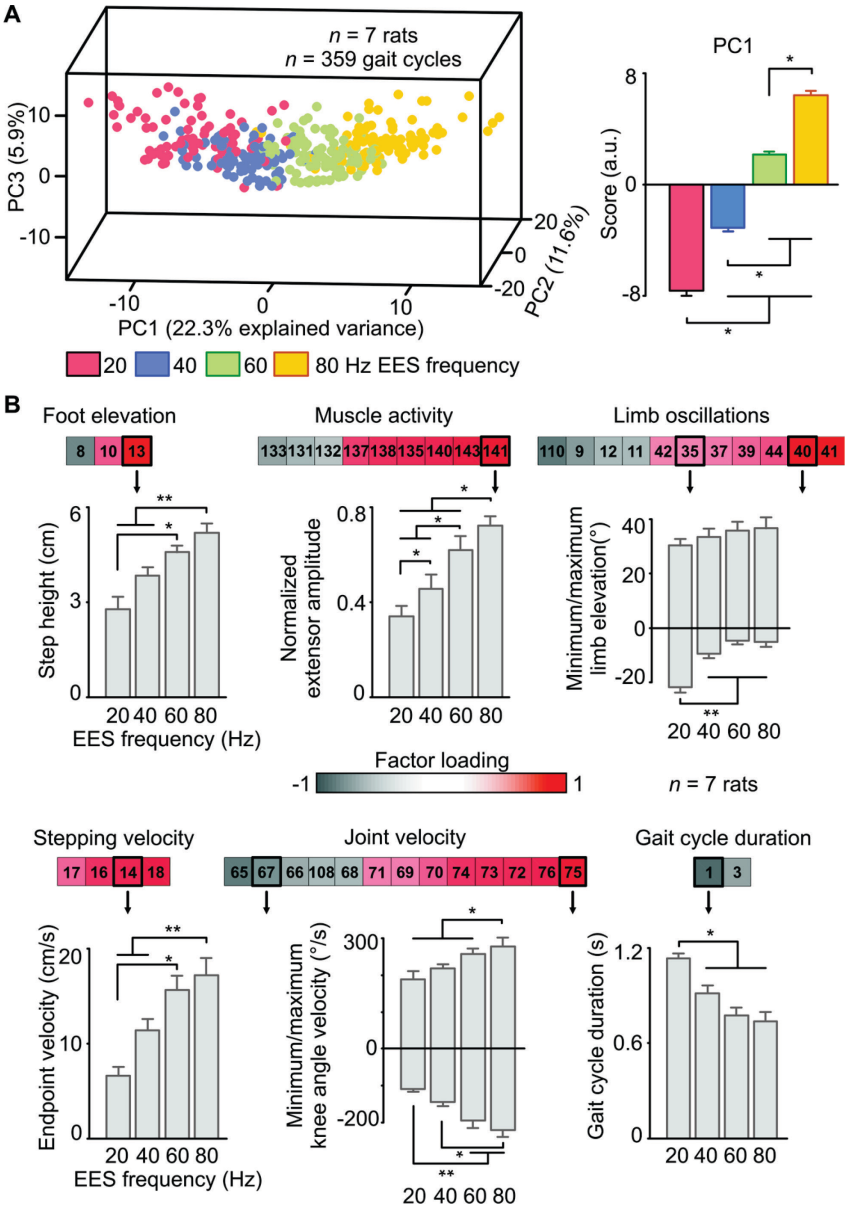

Fig. S2: Modulation of EES frequency tunes multiple aspects of gait patterns. (A) PC analysis applied on all 147 computed parameters (table S1) from all the gait cycles recorded in 7 rats for EES frequencies set at 20, 40, 60, and 80 Hz. Each data point is a gait cycle represented in the 3D space defined by PC1 to PC3. **(B)** Histogram plots reporting the mean values of scores on PC1 for the various EES frequencies. The variables with high factor loadings on PC1 (lvaluel > 0.5) were grouped into functional clusters. Numbers refer to the computed variables in table S1. The histogram plots report, for each functional cluster, the mean values of a representative variable at the different EES frequencies. The arrows refer to the variable illustrated in the histogram plots. Data are means ± SEM. **P*<0.05, ***P*<0.01, Repeated measure ANOVA followed by Newman-Keuls post-hoc tests.

.

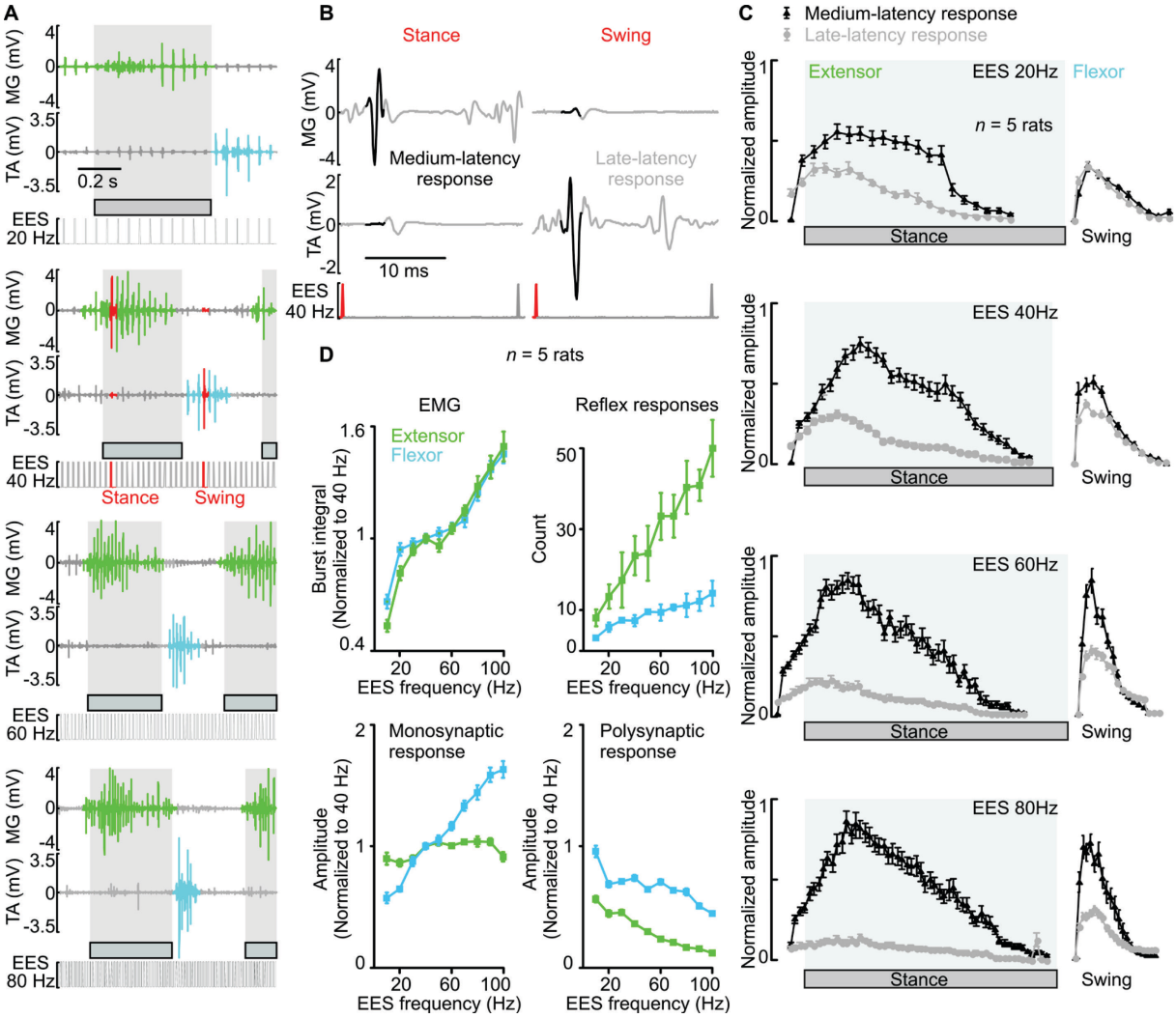

Fig. S3: Modulation of EES frequency tunes mono- and polysynaptic responses in flexor and extensor muscle during locomotion. (A) EMG activity recorded in extensor (MG) and flexor (TA) muscles during a representative gait cycle under EES frequencies set at 20, 40, 60, and 80 Hz. The bursts of EMG activity extracted for further analysis are represented in green and blue for extensor and flexor muscles, respectively. **(B)** Color-coded medium-latency and late-latency reflex responses elicited in extensor and flexor muscles in response to a pulse of EES during stance and swing. Responses are identified based on their respective latencies. The example is extracted from panel (A) during EES at 40 Hz. (**C**) Mean amplitude (± SEM) of each EES-induced monosynaptic (black) and polysynaptic (grey) response over the course of the stance phase for extensor muscles and swing for flexor muscles. EMG bursts were built from a succession of modulated monosynaptic and polysynaptic responses. Ten EMG bursts were analyzed per muscle, condition, and rat (n = 5). The amplitude of responses was normalized to the maximum amplitude recorded for each rat over all the experimental conditions. **(D)** Mean values (± SEM) of EMG burst integrals, of the total number of induced motor responses per burst, and of the averaged amplitude of monosynaptic and polysynaptic responses over the entire bursts in extensor and flexor muscles for the different EES frequencies. Data are for n = 5 rats.

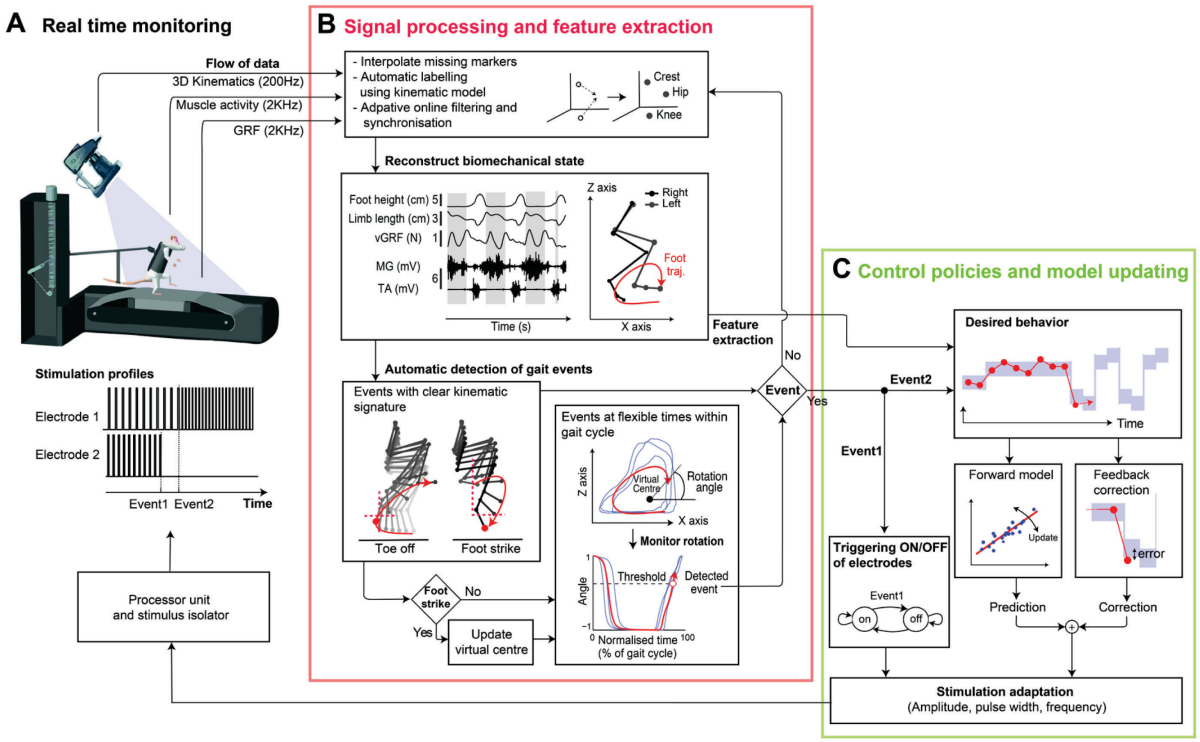

Fig. S4: Real-time monitoring and control platform. (**A**) The flow of kinematics, EMG, and kinetic information was continuously monitored in real-time through the integrated system Vicon. (**B**) All the signals were filtered online using adaptive filters (least mean squares). To deal with missing kinematic information owing to occlusion of markers, the coordinates of each marker were interpolated by triangulation. The different sources of information were synchronized to reconstruct the complete biomechanical state of the locomotor system. The signal-processing system then combined two complementary algorithms to automatically detect key gait events and extract meaningful features integrated into control policies. First, gait events with clear-cut kinematic signatures (foot strike and toe off,) were detected online based on a threshold of foot elevation in the sagittal plane. Second, custom-made algorithms monitored the circular trajectory of the foot around a virtual center updated after each cycle. The rotation angle of the foot trajectory along this circular path allowed to trigger stimulation or updated features of stimulation at any time of the gait cycle. (**C**) Both sets of events triggered controller calculations, which derived the appropriate corrections of EES parameters. The combination of feedback and feed-forward information generated corrections of EES frequency in order to achieve a desired locomotor output. Forward models were automatically updated after each gait cycle to account for putative time-varying characteristics of the system. Each electrode may also be turned on and off at specific times within the gait cycle to reinforce specific aspects of locomotion.

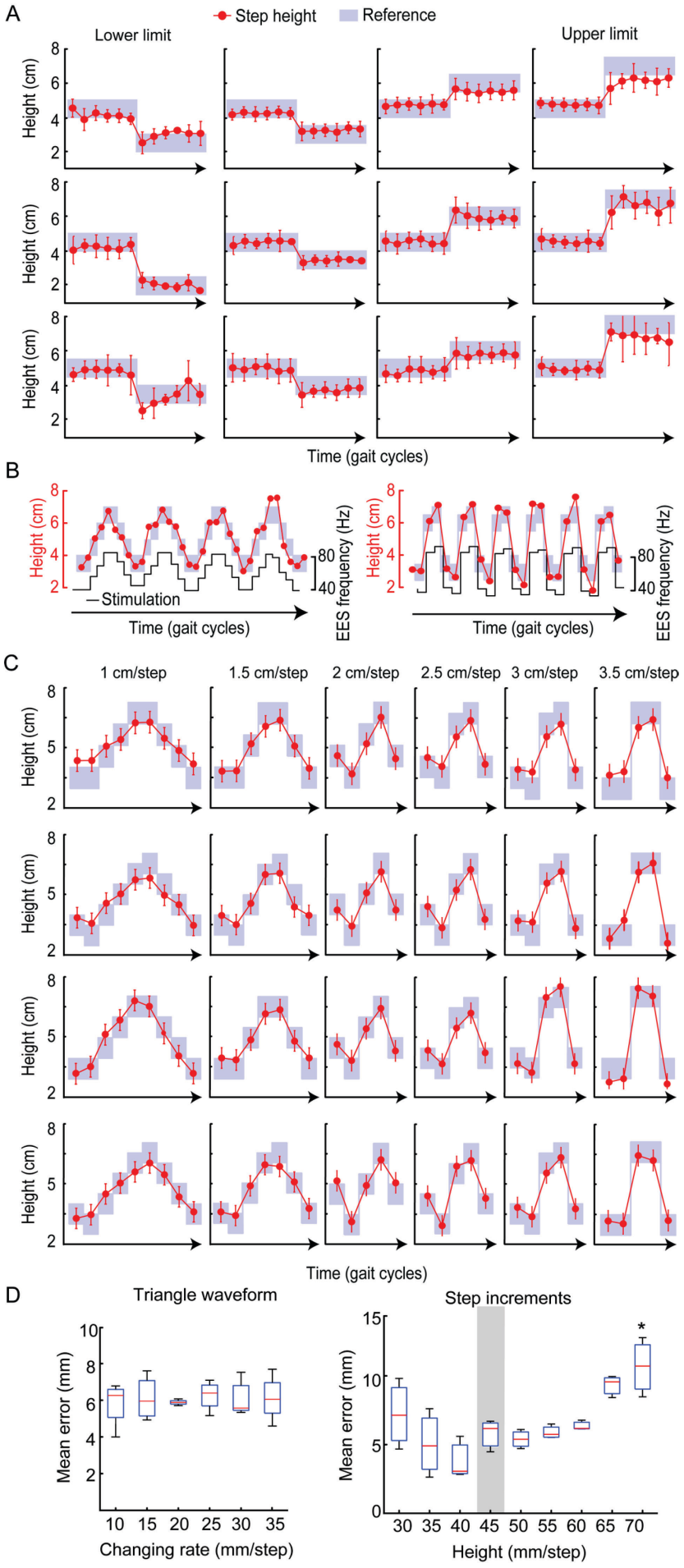

Fig. S5: High-fidelity control of complex foot trajectory. (**A**) Step-increments. Data are mean step heights (± SD) during stepping with constant-shift of the reference band upward or downward with small and large increments/decrements until reaching steady-state (6 consecutive steps). Each horizontal panel corresponds to a distinct rat (n = 3). (**B**) Representative trials showing the step height performance during a tracking task of a periodic triangular waveform (piecewise linear increments or decrements at different rates) during stepping on a treadmill. (**C**) Triangle waveforms. Mean values of step heights (± SD) during the same type of executions shown in (B), but for the entire range of tested increment/decrement values, from left to right. Each horizontal panel corresponds to a distinct rat (n = 4 rats shown). (**D**) Boxplots reporting the median value, SD, and 95% confidence intervals for step height errors for each experimental condition. *P < 0.05 for the marked condition versus all the other conditions (Kruskal-Wallis test).

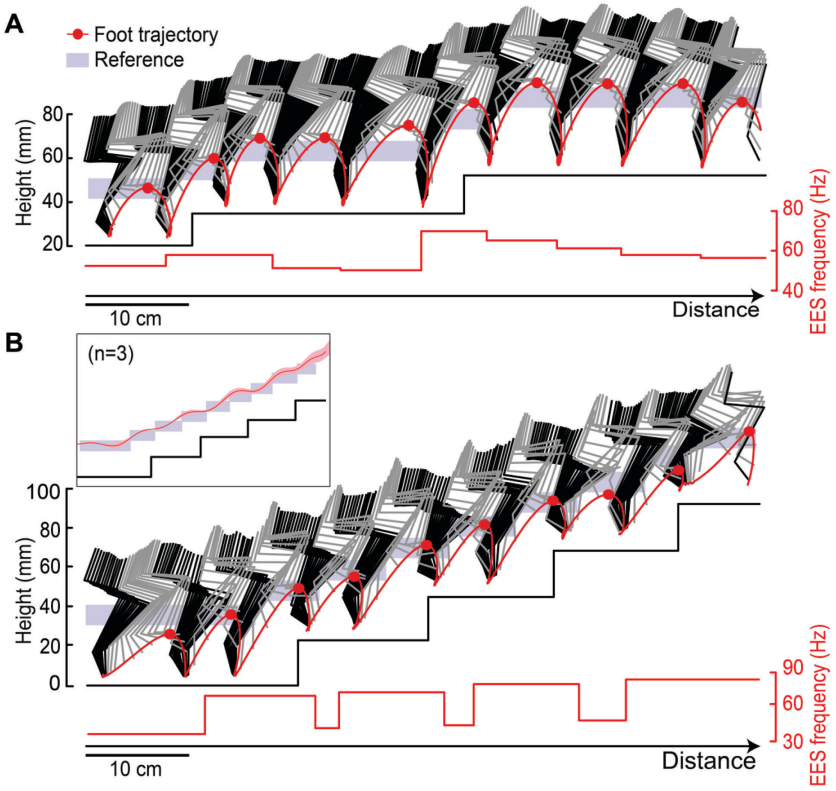

Fig. S6: Execution along staircases of various heights and lengths. (**A**) Representative stick diagram decomposition of hindlimb movement and limb endpoint trajectory during stance (black) and swing (grey) while walking along a succession of two staircases (1.7-cm height, 25-cm length) under controlled condition. The red dots indicate the maximum elevation of the foot during swing, defined as step height. The positions of the reference band and changes in EES frequency are represented by the shaded area and red signal, respectively. (**B**) Same representation as in (A) for an execution along a succession of 4 staircases (2-cm height, 12-cm length). The inset displays the mean foot trajectories (± SD) averaged over 20 successive repetitions for 3 rats.

SUPPLEMENTARY TABLE

Table S1: List of computed kinematic, kinetic, and EMG parameters.

Parameters	Parameter number	Detailed explanation
		Kinematics
Temporal features		
	1	Cycle duration
	2	Cycle velocity
	3	Stance duration
	4	Swing duration
	5	Relative stance duration (percent of the cycle duration)
Limb endpoint (Metatarsal phalange) trajectory		
	6	Interlimb temporal coupling
	7	Duration of double stance phase
	8	Stride length
	9	Step length
	10	3D limb endpoint path length
	11	Maximum backward position
	12	Minimum forward position
	13	Step height
	14	Maximum speed during swing
	15	Relative timing of maximum velocity during swing
	16	Acceleration at swing onset
	17	Average endpoint velocity
	18	Orientation of the velocity vector at swing onset
	19	Dragging
	20	Relative dragging duration (percent of swing duration)
Stability		
Base of support	21	Positioning of the foot at stance onset with respect to the pelvis
	22	Stance width
Trunk and pelvic	23	Maximum hip sagittal position
	24	Minimum hip sagittal position
position and	25	Amplitude of sagittal hip oscillations
	26	Variability of sagittal crest position
oscillations	27	Variability of sagittal crest velocity
	28	Variability of vertical hip movement
	29	Variability of sagittal hip movement
	30	Variability of the 3D hip oscillations
	31	Length of pelvis displacements in the forward direction
	32	Length of pelvis displacements in the medio-lateral direction
	33	Length of pelvis displacements in the vertical direction
	34	Length of pelvis displacements in all directions
Joint angles and segmental oscillations		
Backward	35	Crest oscillations
	36	Thigh oscillations
	37	Leg oscillations
	38	Foot oscillations
	39	Whole limb oscillations
Forward	40	Crest oscillations
	41	Thigh oscillations
	42	Leg oscillations
	43	Foot oscillations
	44	Whole limb oscillations
Flexion	45	Hip joint angle
	46	Knee joint angle
	47	Ankle joint angle
Abduction	48	Whole limb abduction
	49	Foot adbduction
Extension	50	Hip joint angle

	51	Knee joint angle
	52	Ankle joint angle
Adduction	53	Whole limb adduction
	54	Foot adduction
Amplitude	55	Crest oscillations
	56	Thigh oscillations
	57	Leg oscillations
	58	Foot oscillations
	59	Whole limb oscillations
	60	Hip joint angle
	61	Knee joint angle
	62	Ankle joint angle
	63	Whole limb medio-lateral oscillations
	64	Foot abduction/adduction
Velocity		
Minimum	65	Whole limb oscillation velocity
	66	Hip joint angle velocity
	67	Knee joint angle velocity
	68	Ankle joint angle velocity
Maximum	69	Whole limb oscillation velocity
	70	Hip joint angle velocity
	71	Knee joint angle velocity
	72	Ankle joint angle velocity
Amplitude	73	Whole limb angle velocity
	74	Hip joint angle velocity
	75	Knee joint angle velocity
	76	Ankle joint angle velocity
Inter-limb coordination		
PC analysis	77	Degree of linear coupling between joint oscillations
FFT	78	Temporal coupling between crest and thigh oscillations
decomposition	79	Temporal coupling between thigh and leg oscillations
	80	Temporal coupling between leg and foot oscillations
	81	Correlation between crest and tight oscillations
	82	Correlation between tight and leg oscillations
	83	Correlation between leg and foot oscillations
Crosscorrelation	84	Correlation between hip and knee oscillations
	85	Correlation between knee and ankle oscillations
	86	Correlation between ankle and MTP oscillations
	87	Temporal lag between backward positions of crest and thigh oscillations
	88	Temporal lag between forward positions of crest and thigh oscillations
Relative coupling	89	Temporal lag between backward positions of thigh and leg oscillations
	90	Temporal lag between forward positions of the thigh and leg oscillations
	91	Temporal lag between backward positions of leg and foot oscillations
	92	Temporal lag between forward positions of leg and foot oscillations
	93	Lag of the cross correlation function between hindlimb oscillations
Inter-segmental coordination compared to Able-bodied rats	94	Maximum R-value of the cross correlation function between hindlimb oscillations
	95	Lag of the cross correlation function between hip oscillations
	96	Maximum R-value of the cross correlation function between hip oscillations
	97	Lag of the cross correlation function between knee oscillations
	98	Maximum R-value of the cross correlation function between knee oscillations

	99	Lag of the cross correlation function between ankle oscillations
	100	Maximum R-value of the cross correlation function between ankle oscillations
	101	Lag of the cross correlation function between endpoint oscillations
	102	Maximum R-value of the cross correlation function between endpoint oscillations
	103	Phase of the first harmonic of the FFT of the hip elevation angle
	104	Amplitude of the first harmonic of the FFT of the hip elevation angle
	105	Phase of the first harmonic of the FFT of the knee elevation angle
	106	Amplitude of the first harmonic of the FFT of the knee elevation angle
	107	Phase of the first harmonic of the FFT of the ankle elevation angle
	108	Amplitude of the first harmonic of the FFT of the ankle elevation angle
Left–right	109	Phase of the first harmonic of the FFT of the endpoint elevation angle
hindlimb	110	Amplitude of the first harmonic of the FFT of the endpoint elevation angle
coordination	111	Phase of the first harmonic of the FFT of the hindlimb elevation angle
	112	Amplitude of the first harmonic of the FFT of the hindlimb elevation angle
	113	Lag of the cross correlation function between crest and thigh limb elevation angles
Hindlimb	114	Lag of the cross correlation function between thigh and hindlimb elevation angles
coordination	115	Lag of the cross correlation function between hip and thigh elevation angles
	116	Lag of the cross correlation function between hindlimb and foot elevation angles
	117	Lag of the cross correlation function between thigh and ankle elevation angles
	118	Lag of the cross correlation function between ankle and foot elevation angles

Kinetics		
	119	Medio-lateral forces
	120	Anteroposterior forces
	121	Vertical forces
	122	Weight-bearing level

EMG		
Timing (relative to cycle duration, paw contact to paw contact)		
Extensor ipsilateral	123	Relative onset of ipsilateral MG EMG burst
	124	Relative end of ipsilateral MG EMG burst
Flexor ipsilateral	125	Relative onset of ipsilateral TA EMG burst
	126	Relative end of ipsilateral TA EMG burst
Extensor contralateral	127	Relative onset of contralateral MG EMG burst
	128	Relative end of contralateral MG EMG burst
Flexor contralateral	129	Relative onset of contralateral TA EMG burst
	130	Relative end of contralateral TA EMG burst
Duration		
Extensor ipsilateral	131	Duration of ipsilateral MG EMG burst
Flexor ipsilateral	132	Duration of ipsilateral TA EMG burst
Extensor contralateral	133	Duration of contralateral MG EMG burst

Flexor contralateral	134	Duration of contralateral TA EMG burst
Amplitude		
Extensor ipsilateral	135	Mean amplitude of ipsilateral MG EMG burst
	136	Integral of ipsilateral MG EMG burst
	137	Root mean square of ipsilateral MG EMG burst
Flexor ipsilateral	138	Mean amplitude of ipsilateral TA EMG burst
	139	Integral of ipsilateral TA EMG burst
	140	Root mean square of ipsilateral TA EMG burst
Extensor contralateral	141	Mean amplitude of contralateral MG EMG burst
	142	Integral of contralateral MG EMG burst
	143	Root mean square of contralateral MG EMG burst
Flexor contralateral	144	Mean amplitude of contralateral TA EMG burst
	145	Integral of contralateral TA EMG burst
	146	Root mean square of contralateral TA EMG burst
Muscle coactivation	147	Co-contraction of flexor and extensor muscle

SUPPLEMENTARY VIDEOS

Movie S1: Real-time monitoring and control platform. The platform to monitor whole-body kinematics, muscle activity, and ground reaction forces in real-time involves an integrated system that interfaces the reconstructed biomechanical state of the rat with control algorithms. Spatial and temporal features of gait are extracted *online* to trigger feedback and feed-forward adjustments of stimulation parameters in order to maintain step height within a desired range. .

Movie S2: Closed-loop neuromodulation achieves high-fidelity control of leg movements. The experimental procedure promoted locomotion in paralyzed rats. We imposed small changes and large changes in step height, as well as maintenance of stable references. The controller successfully tuned stimulation frequency in order to automatically adjust step height.

Movie S3: Closed-loop neuromodulation prevents rapid fatigue during continuous locomotion. We compared the evolution of the stepping patterns and muscle activity during non-controlled and controlled neuromodulation of spinal circuits. After 9 minutes, rats demonstrated a graded decrease in step height because of fatigue, which was corrected under controlled stimulation conditions.

Movie S4: Closed-loop neuromodulation enables locomotion across staircases. Closed-loop neuromodulation allowed the rats to adjust limb kinematic and ground reaction forces in order to restore locomotion across single and combinations of staircases in paralyzed rats. Automated tuning of EES frequency produced adequate foot trajectory to overcome the staircase. By contrast, non-controlled rats were unable to climb the staircase.